Michalowski, R. L. (2001). *Géotechnique* **51**, No. 9, 787–798

Upper-bound load estimates on square and rectangular footings

R. L. MICHALOWSKI*

Limit analysis of square and rectangular rough footings is presented in this paper. All mechanisms of failure considered in the analysis consist of four regions, each characterised by plane deformation. However, the geometry of the mechanisms is three-dimensional. Both continuous deformation and multi-block patterns are considered. A common feature in all mechanisms is truncation of the blocks with conical surfaces. Standard calculations of the work dissipation rate are complex because of the elaborate three-dimensional geometry. However, a theoretical development is shown indicating that the tedious calculations of work dissipation on curved velocity discontinuity surfaces and within the deforming regions of cohesive-frictional soils can be substituted with an integral over the surface of the mechanism. While this method cannot be used easily for soils with an arbitrary distribution of properties, its application is straightforward for homogeneous soils, and it can also be used for layered soils. Calculations of bearing capacity are performed for both square and rectangular footings. It was surprising to find that the least upper-bound estimates of loads on square footings occur for mechanisms with no symmetry with respect to diagonal planes. The results are given in terms of the bearing capacity coefficients, and shape factors applicable as modifiers in the bearing capacity solution for strip footings. As expected, these factors approach unity with an increase in the footing aspect ratio L/B. The factors calculated are typically larger than earlier empirical proposals in the literature.

KEYWORDS: bearing capacity; failure; footings; limit state design/analysis; plasticity; theoretical analysis.

Nous présentons dans cet exposé une analyse limite d'assises grossières de forme carrée et rectangulaire. Tous les mécanismes de rupture pris en compte dans cette analyse sont constitués de quatre régions, chacune étant caractérisée par une déformation plane. Mais la géométrie des mécanismes est tridimensionnelle. Nous étudions la déformation continue et à blocs multiples. Tous ces mécanismes ont une caractéristique commune: la troncature des blocs avec surfaces coniques. Les calculs standard du taux de dissipation du travail sont complexes en raison de la géométrie tridimensionnelle. Cependant, nous donnons un développement théorique indiquant que les longs calculs de dissipation sur superficie de discontinuation à vélocité courbe et dans les régions de déformation des sols cohésifs-frictionnels peuvent être remplacés par une intégrale sur la surface du mécanisme. Bien que cette méthode ne puisse être utilisée facilement pour les sols ayant une distribution arbitraire des propriétés, son application est simple pour les sols homogènes et elle peut être utilisée aussi pour les sols stratifiés. Nous avons fait les calculs de capacité porteuse pour les assises carrées et les assises rectangulaires. Nous avons été surpris de constater que les évaluations les plus basses de limite supérieure pour les charges sur assises carrées se produisent pour les mécanismes sans symétrie par rapport aux plans diagonaux. Nous donnons les résultats en termes de coefficients de capacité porteuse et de facteurs de forme applicables comme agents modifiants dans la solution de capacité porteuse pour les assises en bandes. Comme on pouvait s'y attendre, ces facteurs approchent de l'unité avec une augmentation du rapport d'élancement de l'assise L/B. Les facteurs calculés sont, de manière typique, plus grands que les facteurs empiriques proposés précédemment dans la documentation.

INTRODUCTION

Design of foundation footings involves settlement and bearing capacity calculations, the latter typically using some form of limit state method. Bearing capacities of square and rectangular footings are usually designed based on a plane-strain solution for a strip (infinite length) footing (Prandtl, 1920; Reissner, 1924), with some empirical modifications to compensate for the finite length. Early attempts included Terzaghi's coefficients for circular and square footings, independent of the soil internal friction angle (Terzaghi, 1943). Shape adjustments to the strip footing solution were later proposed by Meyerhof (1963), De Beer (1970) and Hansen (1970). All these variations of 'shape factors' originate, to some degree, from empirical results.

The kinematic approach of limit analysis is used in this paper to obtain solutions to the bearing capacity of rough rectangular footings. The primary difficulty in this approach is in the complexity of the mechanisms that can describe the process of failure reasonably well. Earlier rigorous limit analysis solutions to three-dimensional bearing capacity problems include primarily frictionless materials (e.g. Shield & Drucker, 1953) for which the collapse mechanisms are not as complex as those for frictional soils.

Manuscript received 6 November 2000; revised manuscript accepted 4 July 2001.
Discussion on this paper closes 1 May 2002, for further details see inside back cover.
* Department of Civil and Environmental Engineering, University of Michigan, USA.

The complexity of the geometry of three-dimensional mechanisms with dilation of soil makes it difficult to construct admissible velocity patterns, and makes calculations of volumes of blocks and areas of discontinuity surfaces quite elaborate. While simple trigonometric treatment of geometry suffices for plane-strain solutions, three-dimensional calculations require that three-dimensional analytical geometry be employed.

To make the computations more tractable, a theoretical development is shown first which makes it possible to avoid complex integration of the work dissipation rate within the deforming soil. Next, three-dimensional mechanisms of collapse are described. The computational results are presented in the penultimate section, and the paper concludes with a discussion and some final remarks.

CALCULATIONS OF THE RATE OF WORK DISSIPATION

One of the difficulties in limit analysis of three-dimensional problems is integrating the rate of work dissipation in continually deforming regions, and on velocity discontinuities that may assume the shape of non-planar surfaces. It is shown in this section that the total dissipation in the entire mechanism can be obtained without detailed integration of the work dissipation on all velocity discontinuity surfaces and within the deforming regions.

We assume that the soil conforms to the Mohr–Coulomb yield condition and the deformation is governed by the normality rule. The rate of work dissipation per unit volume of soil can thus be written as (Drucker & Prager, 1952)

$$\dot{D} = (\dot{\varepsilon}_1 - \dot{\varepsilon}_3)c\cos\varphi \tag{1}$$

where $\dot{\varepsilon}_1$ and $\dot{\varepsilon}_3$ are the major and minor principal strain rates, and c and φ are the cohesion and the internal friction angle of the soil respectively. The associative flow rule implies that a kinematically admissible deformation field conforms to the following relation:

$$\frac{\dot{\varepsilon}_v}{\dot{\gamma}_{max}} = \frac{\dot{\varepsilon}_1 + \dot{\varepsilon}_3}{\dot{\varepsilon}_1 - \dot{\varepsilon}_3} = -\sin\varphi \tag{2}$$

where $\dot{\varepsilon}_v$ is the rate of volumetric strain, and $\dot{\gamma}_{max}$ is the rate of the maximum distortion angle (or double the maximum shear strain rate). Although three-dimensional mechanisms will be considered, they will be assembled from regions with planar deformation: therefore a case where $\dot{\varepsilon}_2 = 0$ is considered here. Now, substituting equation (2) into equation (1), we obtain

$$\dot{D} = -\dot{\varepsilon}_v c\cot\varphi = -(\dot{\varepsilon}_1 + \dot{\varepsilon}_3)c\cot\varphi \tag{3}$$

The expression in equation (3) indicates that the rate of work dissipation can be expressed as a function of the volumetric strain rate (this dissipation rate is always positive, since, according to the compression-plus sign convention, the dilatant volumetric strain rate is negative). Velocity discontinuities can be regarded as finite-thickness layers, and the rate of work dissipated on discontinuity surfaces follows from equation (1) (or equation (3)) integrated over the thickness of the layers. Once the velocity jump vector is given, the result of integration of dissipation becomes independent of the thickness of the layer. Considerations here are therefore restricted to dissipation within continually deforming soil without loss of generality.

The kinematic approach of limit analysis is based on the theorem that states that, in any kinematically admissible mechanism, the rate of work dissipation is not less than the work rate of external forces. The limit load is then calculated from an energy rate balance equation in which all terms represent the global (integrated) rates. The rate of dissipation in equation (3) is directly dependent on the rate of volume change. Therefore the total work dissipation in the mechanism must be uniquely determined by the rate of the volume change in the entire mechanism. Hence, if this volume change could be calculated in some manner, one could avoid tedious calculations of the energy dissipation rate in all deforming regions of the mechanism. A method for such calculations is shown in the next paragraph.

Using the divergence theorem, the integral of the volumetric strain rate in the entire volume V of the mechanism can be presented as an integral over the surface S bounding the extent of the mechanism:

$$\int_V (\dot{\varepsilon}_1 + \dot{\varepsilon}_2 + \dot{\varepsilon}_3)\,\mathrm{d}V = -\int_V \left(\frac{\partial v_1}{\partial x_1} + \frac{\partial v_2}{\partial x_2} + \frac{\partial v_3}{\partial x_3}\right)\mathrm{d}V = -\int_V \frac{\partial v_i}{\partial x_i}\,\mathrm{d}V = -\int_S v_i n_i\,\mathrm{d}S \tag{4}$$

where v_i is the velocity vector and n_i is the outward unit vector normal to S. Product $v_i n_i$ yields the component of v_i perpendicular to boundary S. Surface S bounding the mechanism is divided into part S_t where the stress boundary condition is given (surcharge q), and part S_v, where the velocity boundary condition is known (here it is the soil–footing interface, and the surface separating the mechanism from the stationary soil with zero velocity). The volumetric strain rate in the mechanism is then determined uniquely by the rate of displacement of the boundaries, no matter whether the dilatancy occurred within a continually deforming field or on discontinuities. Consequently, the integral of the work dissipation in equation (3) in the entire mechanism becomes

$$\int_V \dot{D}(\dot{\varepsilon}_{ij})\,\mathrm{d}V = -\int_V (\dot{\varepsilon}_1 + \dot{\varepsilon}_3)c\cot\varphi\,\mathrm{d}V = \left(\int_{S_v} n_i v_i\,\mathrm{d}S_v + \int_{S_t} n_i v_i\,\mathrm{d}S_t\right)c\cot\varphi \tag{5}$$

Notice that as long as the stress state is not at a singular point on the Mohr–Coulomb yield condition, the normality rule assures that $\dot{\varepsilon}_2 = 0$. The energy dissipation rate in the entire volume V of the collapse mechanism can thus be calculated as a surface integral, making the computations relatively simple. This method, however, cannot be used for soils without dilation, where the volumetric changes are equal to zero no matter what the rate of shear in the mechanism. Also, it cannot be used easily for soils with an arbitrary distribution of c and φ. With some modifications, however, this method is applicable to layered soils. In this case, the rate of volume change of each layer needs to be calculated independently from equation (4), with V and S now being the volume of a single layer and the surface bounding this layer respectively.

IMPLICATIONS OF LIMIT ANALYSIS FORMULATION

For soils whose deformation is governed by the normality rule, the rate of work dissipation is not less than the work rate of external loads for any kinematically admissible incipient collapse mechanism:

$$\int_V \dot{D}(\dot{\varepsilon}_{ij})\,\mathrm{d}V \geqslant \int_{S_v} p_i v_i\,\mathrm{d}S_v + \int_{S_t} q_i v_i\,\mathrm{d}S_t + \int_V \gamma_i v_i\,\mathrm{d}V \tag{6}$$

The dissipation rate and the work rate of the soil weight (γ_i being the unit weight vector) are integrated over the entire volume V of the mechanism, whereas the work rate of the given boundary stress, q_i, and the limit load, p_i, are integrated over their respective boundaries S_t and S_v. Application of the kinematic approach requires that the collapse mechanism used in the analysis be optimised to obtain the bound closest to the true limit load. In general, for soils whose yielding is governed by the Mohr–Coulomb yield condition, the limit analysis solution to a limit load can be written as the sum of three terms dependent on the stress boundary condition (q), cohesion (c) of the soil, and its weight (γ). This is the direct consequence of the form of inequality (6). We shall try to indicate in this section when a mechanism associated with the minimum solution is independent of the combination of c, q and γ. This has clear consequences for the optimisation process in limit analysis.

Assume that both surcharge q_i and distributed limit load p_i are uniform and perpendicular to the boundaries:

$$p_i = -p\,n_i, \qquad q_i = -q\,n_i \tag{7}$$

where n_i are outward unit vectors normal to the boundary (both q_i and p_i are acting inwards). Substituting equations (5) and (7) into equation (6) and neglecting the weight term ($\gamma = 0$) we obtain

$$\left(\int_{S_v} n_i v_i\,\mathrm{d}S_v + \int_{S_t} n_i v_i\,\mathrm{d}S_t\right)c\cot\varphi \geqslant -p\int_{S_v} n_i v_i\,\mathrm{d}S_v - q\int_{S_t} n_i v_i\,\mathrm{d}S_t \tag{8}$$

Now, solving for p, we obtain the upper bound for the limit load intensity (note that $-\int_{S_v} n_i v_i\,\mathrm{d}S_v$ is a positive quantity):

$$p \leqslant c\left(\frac{\int_{S_t} n_i v_i\,\mathrm{d}S_t}{-\int_{S_v} n_i v_i\,\mathrm{d}S_v} - 1\right)\cot\varphi + q\,\frac{\int_{S_t} n_i v_i\,\mathrm{d}S_t}{-\int_{S_v} n_i v_i\,\mathrm{d}S_v} \tag{9}$$

Both $c\cot\varphi$ and q are constant, and the geometry of the mechanism affects only the integral expressions. It then follows from the form of equation (9) that, when $\gamma = 0$, the geometry of the collapse mechanism yielding the least upper bound to load intensity p for special cases where either $q = 0$ or $c = 0$ must be the same as that for the case where both $q > 0$ and $c > 0$ (in all cases a minimum of the same integral expression is sought). This conclusion would not have been true, however, if either p_i or q_i (or both) were not normal to the boundary (unit vector n_i in equation (7) would not be the same as that in

equation (5)). This conclusion also would not be true when $\gamma > 0$.

The result in equation (9) is identical to that which follows from a transformation rule proposed by Caquot (1934), applied to a solution for a purely frictional soil (often referred to as the *theorem of corresponding states*). However, the derivation here clearly indicates that this rule is applicable only to cases where boundary stresses are perpendicular to the boundary (see also Michalowski, 2001). For this reason the classical solutions to bearing capacity of Prandtl (1920) ($q = 0$) and Reissner (1924) ($c = 0$) are additive, but when $\gamma > 0$ the mechanism associated with a rigorous least upper bound is no longer the same as that associated with the Prandtl static solution (Michalowski, 1997).

THREE-DIMENSIONAL COLLAPSE MECHANISMS

Examples of three-dimensional collapse mechanisms for punch indentation into a frictionless half-space can be found in an early paper by Shield & Drucker (1953). A quasi-steady (self-similar) mechanism was devised for a process of tetrahedral indentation of metals with surprisingly good correlation with experimental tests (Michalowski, 1986). A qualitatively similar three-dimensional mechanism for a frictional material was considered in a problem of rock splitting (Michalowski, 1985). The mechanisms developed here resemble that in the latter paper with two exceptions: (1) an incipient indentation process of a flat footing is now considered rather than a quasi-steady process of tetrahedral penetration, and (2) the mechanism is modified with conical surfaces. This modification introduces computational complexity, but it leads to a much improved (more realistic) mechanism. All mechanisms considered here are for rough footings.

An attempt to truncate a three-dimensional collapse mechanism with conical surfaces was suggested by Murray & Geddes (1987) in a simple one-block uplift mechanism of a rectangular anchor plate. Subsequently, Leca & Dormieux (1990) used conical surfaces in limit analysis of shallow tunnels. More recently, Regenass (1999) used a series of conical surfaces to analyse the pull-out force of circular anchor plates. A new element in this paper is a continuous deformation field with a curved conical surface and also a complex mechanism with a series of blocks rounded with a series of conjugate cones.

Continuous deformation mechanism for square footings

A mechanism with a continuous deformation field is presented first. Figs 1(a) and 1(b) illustrate the view of the mechanisms for a square footing, for relatively large and small internal friction angles respectively. This mechanism consists of an inverted rigid pyramid underneath the footing and four deformation regions extending from the four flanks of the pyramid. A portion of the mechanism adjacent to one side of the square footing is shown in Fig. 2(a). Volume $T'ST''RO_1$ has the shape of a curvilinear cone with an apex angle of 2φ. This cone is generated by a series of linear cones with circular directrices. Surface $A'O_1T'A'$ (and $A''O_1T''A''$) is tangent to the cone along O_1T' (and O_1T''). A vertical cross-section of this mechanism is presented in Fig. 2(b). Line $O_1O_2O_3$ is a geometrical location of apex points of linear cones generating the non-linear cone. Lines S_2S_3 and R_2R_3 are straight segments of the generatrix of the linear cone (with apex at O_3). This cone is tangent to the non-linear cone and it has an elliptical cross-section with the soil surface (S_3R_3). Block $A'B'B''A''O_1$ moves vertically down with velocity v_0. Surface $A'A''O_1$ is a velocity discontinuity with velocity jump magnitude of $[v]$ (Fig. 2(c)). Line O_1SS_2 (Fig. 2(b)) is a segment of log spiral

$$r = r_0 \, e^{\theta \tan \varphi} \tag{10}$$

while ORR_2 is a segment of log spiral

$$r = r_0 \, e^{-\theta \tan \varphi} \tag{11}$$

where r_0 is equal to distance AO_1 and θ is shown in Fig. 2(b).

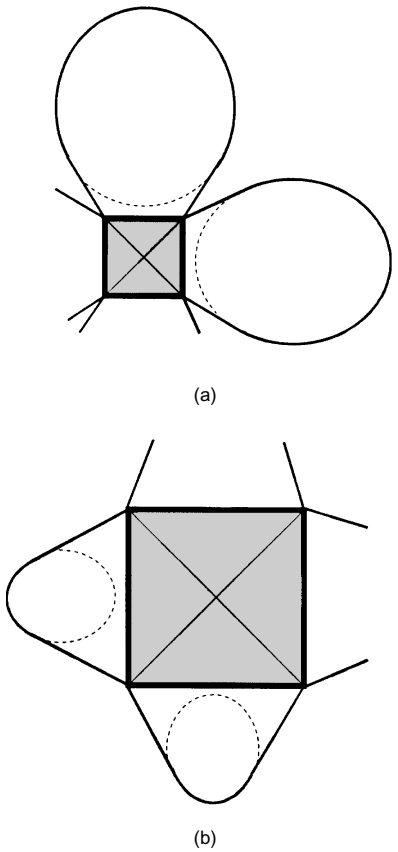

Fig. 1. Collapse mechanisms for square footings: (a) large internal friction angle; (b) small φ

The shaded area $RT'ST''$ in Fig. 2(a) is a circular cross-section of the non-linear cone. It is also a cross-section of the linear cone with apex at O_2 in Fig. 2(b). This cone has an apex angle of 2φ, so that a vector directed along the cone axis is inclined at φ to the cone generatrix.

The velocity field in any radial cross-section (originating at A, Fig. 2(b)) between AO_1 and AS_2 is uniform, and the magnitude of the velocity can be calculated from

$$v = v_1 \, e^{\theta \tan \varphi} \tag{12}$$

which is illustrated in the hodograph (Fig. 2(c)).

Each quarter of the mechanism is separated from the soil at rest by a portion of the curvilinear cone surface (with apex at O_1, Fig. 2), a portion of a linear cone surface (with apex at O_3), and surfaces generated by radii originating at point A' (and A'') and tangent to those cones. The trace of the mechanism on the soil surface is a portion of an ellipse and two straight segments tangent to that ellipse (Fig. 1).

Deformation within each fourth of the mechanism is plane in the sense that there is no out-of-plane velocity component, but the geometry of the failure pattern is three-dimensional. Equation (2) is satisfied everywhere in the strain-rate field. The velocity vectors at discontinuity surfaces separating the deformation field from the material at rest are inclined at angle φ to these surfaces: thus they preserve the kinematical admissibility of the deformation field. However, integrating the energy dissipation rate over the curved discontinuity surfaces in this mechanism (and in the continual deformation region) would have been a complex task, and the benefit of equation (5) now becomes evident. Computational results will be shown later in this paper.

Multi-block mechanism

The multi-block mechanism described in this section is conceptually similar to the continuous mechanism. The region

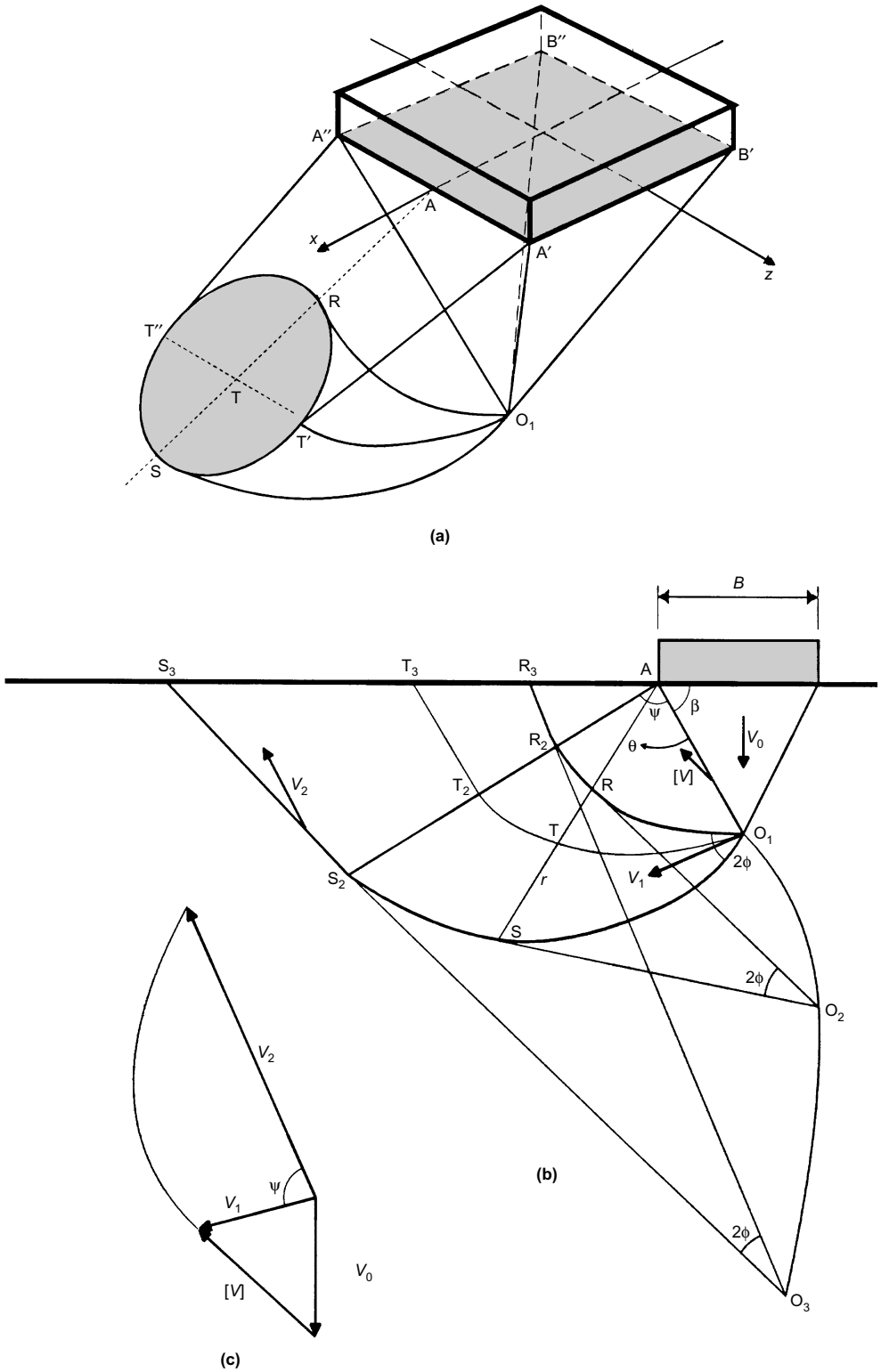

Fig. 2. Collapse of soil under a square footing: (a) mechanism with continuous deformation; (b) vertical cross-section; (c) hodograph

of continuous deformation is now divided into a series of rigid blocks. A portion of the mechanism consisting of a pyramid and two subsequent blocks is shown in Fig. 3(a). The pyramidal block immediately underneath the footing moves vertically down. The block adjacent to this pyramid is a tetrahedron truncated by a cone with apex at O_1 and with an elliptical directrix (the smaller ellipse in Fig. 3(a)). The next block is another tetrahedron truncated by a conical surface with apex at O_2, and the subsequent blocks (not shown) are similar. All conical surfaces have an apex angle of 2φ. A projection of this mechanism on the vertical plane is shown in Fig. 3(b).

Each block moves as a rigid body with a velocity determined in the hodograph in Fig. 3(c). The direction of the velocity for each block coincides with the axis of its respective cone. A typical block is separated from the soil at rest with two planar surfaces (such as $A'T_2'T_3'A'$) and a segment of a conical surface (such as that below points T_2' and T_3', Fig. 3(a)). Line segment $T_2'T_3'$ represents the geometrical location of points where the plane segment is tangent to the conical surface. Blocks are separated from one another by triangular discontinuity surfaces truncated by ellipses (such as $A'T_2'S_2T_2''A''$).

Cones associated with two adjacent blocks intersect the plane

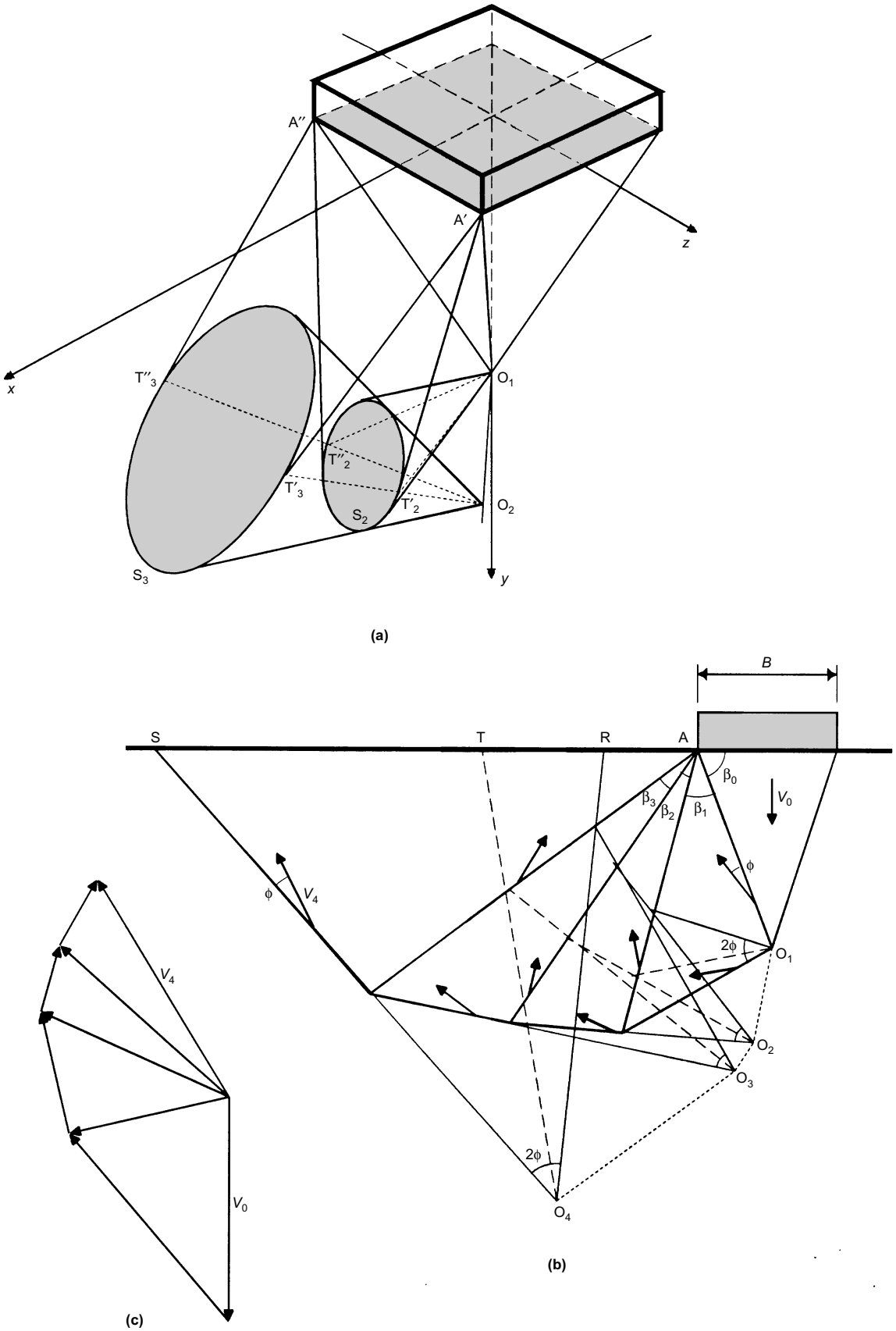

Fig. 3. Multi-block failure pattern: (a) rigid blocks; (b) vertical cross-section; (c) hodograph

that separates these blocks. The kinematical admissibility of the mechanism requires that the traces of both cones on the interface plane coincide. This leads to a significant constraint on the geometry of the three-dimensional mechanism; it is illustrated in Fig. 4. Once orientation of the cone with apex at O_1 is selected and angle β_1 is given, orientation of the subsequent cone (with apex at O_2) is uniquely determined. Apex O_2 must be located on line O_1O_2, parallel to cross-section R_2S_2. Triangle $R_2O_2S_2$ must be a mirror image of triangle $R_2O_1S_2$. Only then will the elliptical cross-section R_2S_2 of the cone with an apex

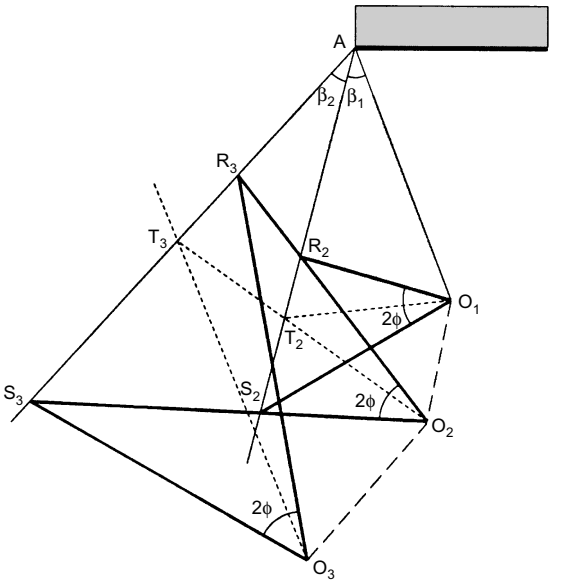

Fig. 4. Admissibility requirement for blocks truncated with conical surfaces

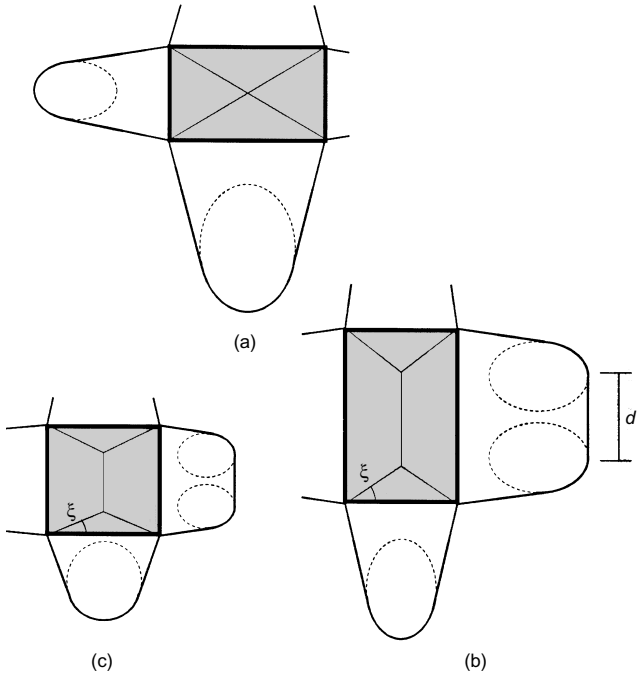

Fig. 5. Failure patterns for (a), (b) rectangular and (c) square footings

at O_1 coincide with the ellipsoidal cross-section R_2S_2 of the cone with an apex at O_2. This has significant consequences for the process of optimisation of the mechanism, where only angles β_i for rigid blocks are variable parameters, whereas inclination of the cones is not variable. This is quite different from plane-strain mechanisms. Notice that with an increase in the number of blocks, contour $S_2S_3 \ldots S_n$ approaches a log spiral. Some details of the computations will be described later in this paper.

Presentation of all the equations used in the analysis of geometry of this mechanism would be unreasonable; however, some indication as to how the mechanism was constructed is given in Appendix 1.

Rectangular footings

The mechanisms for a square footing considered in the previous sections had four vertical planes of symmetry. The rigid-block pattern was generalised for rectangular footings according to the schematic in Figs 5(a) and 5(b), both with two planes of symmetry. The continuous field mechanism was not generalised for rectangular footings, as the calculations for square footings revealed that it does not yield the least upper bound of all mechanisms considered.

The first mechanism in Fig. 5 is a straightforward extension of the mechanism for a square footing. The second one is similar to the first one, with a plane-strain section (of width d) inserted in the central part, as shown in Fig. 5(b). The block underneath the footing in this mechanism has the shape of an inverted roof structure. It was found out from computations that the least upper bound was typically associated with the latter mechanism. It was also interesting to find out that, even for square footings, the pattern in Fig. 5(c) led to a better (lower) limit load than the patterns with four planes of symmetry in Fig. 1.

COMPUTATIONAL RESULTS

Because of the complexity of the geometry of the mechanisms involved, no closed form solutions for the terms in inequality (6) were attempted. Numerical calculations involved three-dimensional analytical geometry and trigonometry, and some details are presented in Appendix 1. Calculations for each mechanism involved optimisation of the geometry so that the least upper bound for the bearing capacity was obtained. The variables in the optimisation procedure were independent angles describing the geometry of mechanisms. These angles were varied with a minimum step of 0·3°.

Calculations have been performed first for footings on weightless soil. The intensity of the bearing pressure is traditionally presented as the sum of components dependent on the soil cohesion and surcharge load:

$$p = cN'_c + qN'_q \tag{13}$$

where N'_c and N'_q are coefficients for rectangular footings. Both p and q are perpendicular to the boundary, and therefore the structure of equation (13) must be the same as that in inequality (9): hence

$$p = c(N'_q - 1)\cot\varphi + qN'_q \tag{14}$$

Based on the form of inequality (9), it was proved that (in the absence of soil weight) coefficients N'_c and N'_q are only functions of the internal friction angle. For convenience, these coefficients can be written as functions of coefficients N_c and N_q for strip footings:

$$N'_c = s_cN_c, \qquad N'_q = s_qN_q \tag{15}$$

where N_c and N_q are coefficients for a strip footing (here, a three-dimensional solution for $L/B = 25$ will be used), and s_c and s_q are often referred to as shape factors. Now considering that $N'_c = (N'_q - 1)\cot\varphi$, factor s_c can be expressed as a function of s_q:

$$s_c = \frac{s_qN_q - 1}{N_q - 1} = \frac{s_qN_q - 1}{N_c\tan\varphi} \tag{16}$$

Such a method of deriving s_c was proposed by de Beer (1970). However, his suggestion that it holds for the general case when the load is inclined and the soil has weight is not strictly true.

The influence of the soil weight on the bearing capacity of square and rectangular footings is presented as an additional term in equation (13):

$$p = c\,N'_c + q\,N'_q + \tfrac{1}{2}\gamma BN'_\gamma \tag{17}$$

where

$$N'_\gamma = s_\gamma N_\gamma \tag{18}$$

and N_γ is a coefficient for a strip footing. There are several different proposals for N_γ (Meyerhof, 1963; Hansen, 1970; Vesic, 1973; Bolton & Lau, 1993). A strict least upper-bound

solution to N_γ obtained recently (Michalowski, 1997) is shown in Table 1, and it can be described with an approximate closed form:

$$N_\gamma = e^{0{\cdot}66+5{\cdot}11 \tan \varphi} \tan \varphi \quad (19)$$

Along with the least upper bound for a strip footing, a solution based on a three-dimensional multi-block mechanism is presented in the last column of Table 1 ($L/B = 25$, 12 blocks). It is rather surprising that the three-dimensional mechanism for a long footing yields a solution that significantly overestimates the plane-strain analysis. This is an artifact of the three-dimensional analysis presented here, where, compared with plane-strain analysis, the kinematic constraints leave fewer independent parameters with respect to which the mechanism can be optimised (see the section 'Multi-block mechanism' above). Consequently, with increasing L/B the three-dimensional mechanism does not approach the plane-strain pattern. For reasons of consistency of results, N_γ in the last column of Table 1 will be used later to calculate coefficient s_γ for rectangular footings.

Superposition of terms in bearing capacity formula

The superposition rule is not applicable when solving nonlinear problems, and the solutions to the terms in equation (17) cannot be calculated separately unless the mechanisms yielding the least upper bounds for each term are identical (Michalowski, 1997). It was argued recently (Michalowski, 2001) that, using the correspondence rule (Caquot, 1934), static solutions for cohesive-frictional soils can be obtained by modifying solutions for frictional soils only when principal stress trajectories for both solutions coincide (without violating the boundary conditions). Consequently, separately calculated bearing capacity components (dependent on cohesion, overburden and soil weight) become additive (superposition principle holds) only when the principal stress trajectories associated with partial solutions coincide. An extensive treatment of superposition of dissipated work in upper-bound analysis for frictionless materials was presented recently by Puzrin & Randolph (2001).

It appears from equation (9) that only when $\gamma = 0$, and p and q are perpendicular to the boundary, will the mechanism for the first two terms of equation (17) be identical, and the superposition principle applicable. Once the weight of the soil is added, the shape of the mechanism that yields the least upper bound to the bearing capacity becomes dependent not only on φ but also on $c/\gamma B$ and $q/\gamma B$. This was shown earlier for strip footings (Michalowski, 1997), and it is also true for rectangular footings. An example of bearing capacity factors, N', for a rectangular footing is given in Tables 2 and 3. Coefficients N'_c and N'_q vary little with the change in $c/\gamma B$ and $q/\gamma B$, but N'_γ varies significantly.

Despite proof to the contrary, for simplicity of design, coefficients N' in equation (17) are typically taken as functions of φ only. For practical purposes, these coefficients are presented as functions of φ in this paper also. N'_c and N'_q (or s_c and s_q) were calculated assuming $\gamma = 0$, and N'_γ (or s_γ) was computed for $c = 0$ and $q = 0$. The superposition of the terms so calculated can no longer be proved a strict upper bound to the true bearing capacity. However, such a result is acceptable in practice.

Table 1. Coefficient N_γ for rough strip footings (2-D and 3-D limit analysis)

φ: degrees	N_γ†	N_γ‡
0	0	0
5	0·181	0·383
10	0·706	1·100
15	1·938	2.702
20	4·468	6·025
25	9·765	13·739
30	21·394	31·617
35	48·681	76·552
40	118·827	206·497
45	322·835	656·613

† Michalowski, 1997.
‡ 3-D analysis, $L/B = 25$.

Table 2. Rectangular footing: bearing capacity coefficeints, $L/B = 2$, $\varphi = 15°$ (least upper bound)

$\frac{q}{\gamma B}$	$\frac{c}{\gamma B}$	N'_c	N'_q	N'_γ
0	0	–	–	2·654
	1	15·963	–	3.903
	2	16·150	–	4·173
	5	15·669	–	4·655
2	0	–	5·348	3·541
	1	15·988	5·284	4·089
	2	15·878	5·254	4·460
	5	15·688	5·203	4·628

Table 3. Rectangular footing: bearing capacity coefficients, $L/B = 2$, $\varphi = 35°$ (least upper bound)

$\frac{q}{\gamma B}$	$\frac{c}{\gamma B}$	N'_c	N'_q	N'_γ
0	0	–	–	134·184
	1	139·606	–	149·004
	2	139·266	–	151.837
	5	140·927	–	161·917
2	0	–	101·126	147·674
	1	139·978	99·014	149·704
	2	137·489	97·271	155·196
	5	136·220	96·382	156·134

Square footings

Computations of the bearing capacity for square footings were performed using the mechanisms in Fig. 2, Fig. 3, and Fig. 5(c). The results in terms of coefficients N'_c and N'_q ($\gamma = 0$) are given in Table 4.

The continuous mechanism in Fig. 2 was optimised with variable angles β, ψ and an angle describing the inclination of the cone at apex O_1. These three angles fully determine the geometry of the entire mechanism. Calculated coefficients N'_c and N'_q based on this mechanism are given in the second and third column of Table 4.

The number of independent variables for the mechanism in Fig. 3 depends on the number of blocks taken in calculations. Except for the last block, each requires one angle (β) to be specified. The inclination of the first cone (with apex at O_1) was also taken as an independent parameter. While the number of independent parameters fully describing the geometry of the mechanism is fixed, the choice of independent parameters may vary. For convenience, the orientation of the first cone was described by the inclination of the line of intersection of planes $O_1A'T'_2$ and $O_1A''T_2''$, both tangent to that cone (see Appendix 1). Once angles β are specified, the inclination of subsequent cones becomes uniquely determined by the requirement of the kinematical admissibility of the mechanism (Fig. 4). Calculations for the mechanism in Fig. 3 were performed for 11 blocks extending to each of the flanks of the pyramid under the footing. An increase in the number of blocks led to an insignificant improvement of results (less than 1%). The results are shown in Table 4, columns 4 and 5.

The mechanism for square footings with two planes of symmetry (Fig. 5(c)) requires twice the number of independent parameters, with two sets of angles β, one for each symmetric cross-section. Calculations were performed again for 11 blocks in each quarter of the mechanism, and the results are given in Table 4, columns 6 and 7.

It is surprising that the least upper bound to N'_c and N'_q was found for the mechanism with two planes of symmetry, schema-

Table 4. Square footings: bearing capacity coefficients N'_c and $N'_q(\gamma = 0)$

φ: degrees	Continuous mechanism		Multi-block with four planes of symmetry		Multi-block with two planes of symmetry	
	N'_c	N'_q	N'_c	N'_q	N'_c	N'_q
10^{-3}	6·830	1·000	6·823	1·000	6·561	1·000
5	9·544	1·835	9·270	1·811	8·720	1·762
10	14·365	3·532	13·613	3·400	12·665	3·233
15	22·984	7·158	21·617	6·792	19·514	6·228
20	39·199	15·267	36·844	14·410	31·844	12·590
25	71·379	34·284	67·432	32·444	55·155	26·719
30	139·337	81·446	132·711	77·621	104·019	61·055
35	294·373	207·122	283·159	199·270	199·052	140·378
40	685·031	575·809	665·051	559·044	501·278	421·622
45	1807·023	1808·023	1773·316	1774·316	1406·519	1407·519

tically indicated in Fig. 5(c), even though the boundary conditions have four planes of symmetry. The same peculiarity was found earlier for a square punch indentation of metals (Shield & Drucker, 1953).

Rectangular footings

The bearing capacity for rectangular footings presented here is based on a multi-block mechanism schematically indicated in Fig. 5(b). This mechanism provided solutions to coefficients N'_c and N'_q lower than any of the other mechanisms considered. Calculations were performed with 11 blocks extending to each side of the pyramid under the footing. For a given L/B the geometry of this pyramid is given by angle β_0 (Fig. 3(b)) and angle ξ (Fig. 5 (b)). The rest of the mechanism geometry is determined by two sets of angles $\beta_i (i = 1, 2, \ldots, n-1)$ in the two symmetric cross-sections parallel to B and L, and the inclination of the first conical surface in each cross-section. Hence the total number of variables in the optimisation process was $2(n+1)$, where n is the number of blocks extending from each of the four flanks of the pyramid. The number of blocks in the entire mechanism is $4n+1$. Some details of constructing the mechanism are given in Appendix 1.

The results are given in Table 5 in terms of coefficients N'_c and N'_q (calculations for $\gamma = 0$). These coefficients are, of course, functions of the footing aspect ratio L/B, with a strong non-linear effect particularly for large internal friction angles, as indicated by the shape factors in Fig. 6. These shape factors were calculated using definitions in equation (15), with N_c and N_q obtained from calculations for $L/B = 25$.

Separate calculations were made for $\gamma > 0$ (and $c = 0$, $q = 0$) to estimate the influence of the soil weight on the bearing capacity of rectangular footings. As argued earlier, the superposition of separately calculated different components of bearing capacity does not provide a strict upper-bound solution, but it is acceptable for design. Both N'_γ and s_γ are given in Table 6 and Fig. 7. Results are presented for $\varphi \geqslant 10°$. Coefficient N'_γ reaches zero when φ is decreased to zero. For large internal friction of the soil, coefficient s_γ increases rapidly with a decrease in L/B, but for φ less than about 16° coefficient s_γ decreases to magnitudes below 1 with a decrease in L/B. The latter may be of little practical consequence, since N'_γ for small φ becomes negligible when compared with N'_c and N'_q.

DISCUSSION OF RESULTS AND FINAL REMARKS

Rigorous upper-bound solutions to limit loads on square and rectangular footings have been found. These solutions are very strongly dependent on the internal friction of the soil. For large internal friction angles the limit loads (or shape factors) are rapidly increasing when the footing aspect ratio L/B drops down to 1, whereas for small internal friction angles the increase is much smaller. While the tendency in the results is intuitively correct, the magnitudes of the shape factors differ from the proposals available in the literature.

The two most commonly cited proposals for the shape factors are those by Meyerhof (1963) and de Beer (1970). Prior to these two, Terzaghi (1943) suggested that for a square footing coefficients $s_c = 1{\cdot}3$, $s_q = 1$ and $s_\gamma = 0{\cdot}8$ be used. These were based on the tests of Golder (1941) and some additional unpublished data. Coefficient $s_c = 1{\cdot}3$ appears to come from Golder's tests on clay with square and rectangular model footings (calculated as the ratio of the 'ultimate pressure' under 3×3 in (76×76 mm) model footings to the pressure under 18×3 in (457×76 mm) footings). Not surprisingly, $s_c = 1{\cdot}3$ agrees well with the factor calculated by the writer for soils with small internal friction angle (5°) and $L/B = 1$ (Fig. 6(a)).

Coefficient $s_\gamma = 0{\cdot}8$ in Terzaghi's suggestion seems to have been deduced from Golder's experiments on sand with footings 6 in (152 mm) in width, with aspect ratios from 1 to 5. The results had a large scatter, where the least ultimate pressure was obtained for a square footing, but also some of the largest pressures were obtained for square plates. Terzaghi seems to have disregarded the scatter, and took only 'the most unfavorable test results as a basis for establishing a provisional equation' (Terzaghi, 1943). In doing so, Terzaghi also ignored any influence of internal friction on the shape factors. It might be of some interest that, based on the very same experiments,

Table 5. Rectangular footings: bearing capacity factors N'_c and $N'_q(\gamma = 0)$

φ: degrees	$L/B = 1{\cdot}5$		$L/B = 2{\cdot}0$		$L/B = 3$		$L/B = 5$		$L/B = 10$	
	N'_c	N'_q	N'_c	N'_q	N'_c	N'_q	N'_c	N'_q	N'_c	N'_q
10^{-3}	6·192	1·000	6·060	1·000	5·638	1·000	5·489	1·000	5·199	1·000
5	8·087	1·707	7·734	1·676	7·403	1·647	7·023	1·614	6·766	1·592
10	11·474	3·023	10·733	2·892	9·074	2.758	9·363	2·651	8·868	2·563
15	16·901	5·528	15·585	5·176	14·147	4·790	12·932	4·465	12·015	4·219
20	26·182	10.529	23·912	9·545	20·766	8·558	18·493	7·730	16·772	7·104
25	43·637	21·348	38·312	18·865	32·477	16·144	28·123	14·114	24·539	12·443
30	78·971	46·594	67·099	39·739	55·109	32·817	45·846	27·469	38·154	23·028
35	159·528	112·703	132·311	93·645	103·868	73·739	82·031	58·439	64·463	46·138
40	364·521	306·870	294·004	247·698	224·037	188·989	166·329	140·567	121·520	102·968
45	989·041	990·041	776·964	777·964	567·491	568·491	399·837	400.837	271·556	272·556

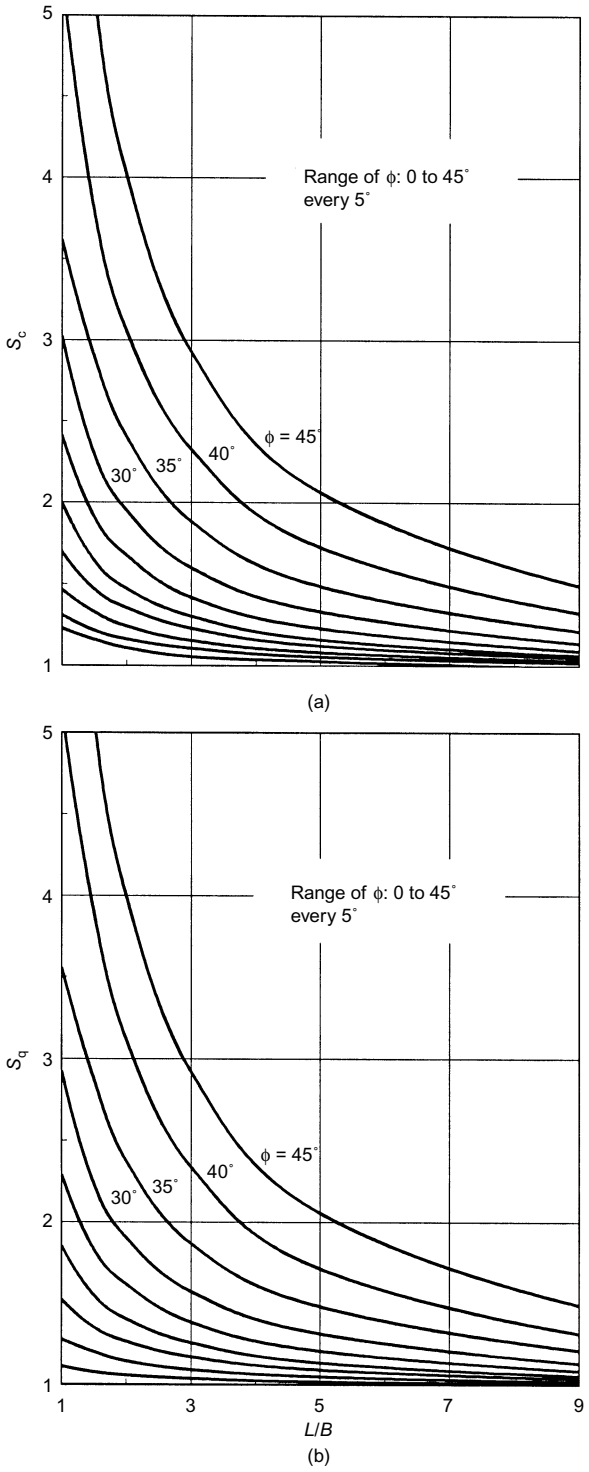

Fig. 6. Shape factors s_c and s_q for rectangular footings

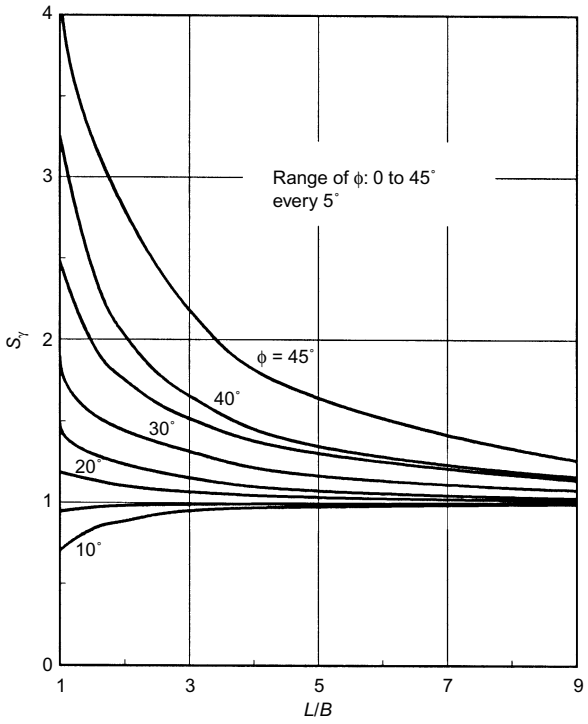

Fig. 7. Shape factor s_γ for rectangular footings

Golder concluded that the footing length does not influence the bearing capacity: 'The maximum pressure on a square footing on sand is equal to that on a long strip of the same width' (Golder, 1941). It is fair to conclude that small-scale testing for influence of the soil weight on the bearing capacity is not likely to be representative of large prototypes (unless a centrifuge is used). However, the trace of the failure mechanism in Golder's experiments very much resembles that in Fig. 1 and Fig. 5. It is interesting to notice that while the limit analysis results show a very rapid increase of s_γ with a decrease in L/B for large φ, the trend is reversed for small φ (Fig. 7).

Both Meyerhof (1963) and de Beer (1970) acknowledge the influence of φ on coefficients s, but the magnitudes of those coefficients differ from those calculated using limit analysis here. While these coefficients are claimed to be 'empirical', no comprehensive test results supporting these proposals were offered. Coefficients s_c proposed by Meyerhof (1963) and de Beer (1970) fall very close to one another, whereas the upper-bound calculations yield larger s_c (Fig. 8(a)). Meyerhof's proposal is the most conservative for both s_c and s_q (Fig. 8(b)).

The proposals for s_γ by Meyerhof and de Beer are rather inconsistent: the former suggests an increase of s_γ with a decrease in L/B (Fig. 9), whereas the latter implies a decrease in s_γ with a decrease in L/B independent of φ (de Beer adopted this proposal after Hansen; see de Beer, 1970). Upper-bound calculations suggest that a trend proposed by de Beer is

Table 6. Bearing capacity factor N'_γ and coefficient $s_\gamma (c = 0, q = 0)$

φ: degrees	$L/B = 1$		$L/B = 1{\cdot}5$		L/B=2·0		$L/B = 3$		$L/B = 5$		$L/B = 10$	
	N'_γ	s_γ	N'_γ	s_γ	N'_γ	s_γ	N'_γ	s_γ	N'_γ	s_γ	N'_γ	s_γ
10	0·778	0·707	0·923	0·838	0·978	0·888	1·046	0·950	1·076	0·977	1·098	0·998
15	2·560	0·947	2·623	0·970	2·654	0·982	2·679	0·991	2·692	0·996	2·699	0·998
20	7·160	1·188	6·878	1·141	6·641	1·102	6·431	1·067	6·246	1·036	6·111	1·014
25	20·399	1·484	17·863	1·300	17·073	1·242	15·873	1·155	14·788	1·076	14·094	1·025
30	59·895	1·894	49·789	1·547	46·203	1·461	41·646	1·317	36·945	1·168	33·756	1·067
35	189·640	2·477	151·367	1·977	134·184	1·752	116·138	1·517	100·130	1·307	85·140	1·112
40	671·694	3·252	502·152	2·431	417·755	2·023	353·455	1·711	279·149	1·351	234·531	1·135
45	2797·328	4·260	2125·806	3·237	1857·524	2·828	1431·868	2·180	1078·989	1·643	787·591	1·199

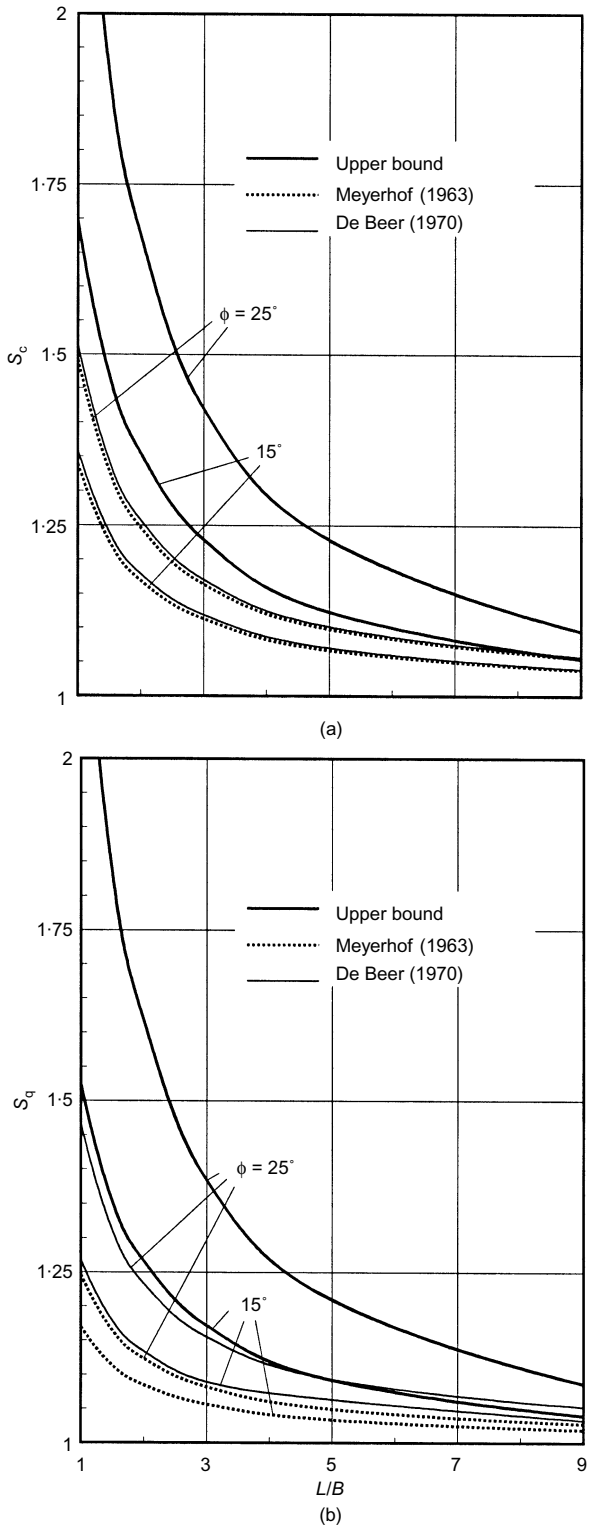

Fig. 8. Comparison of shape factors s_c and s_q

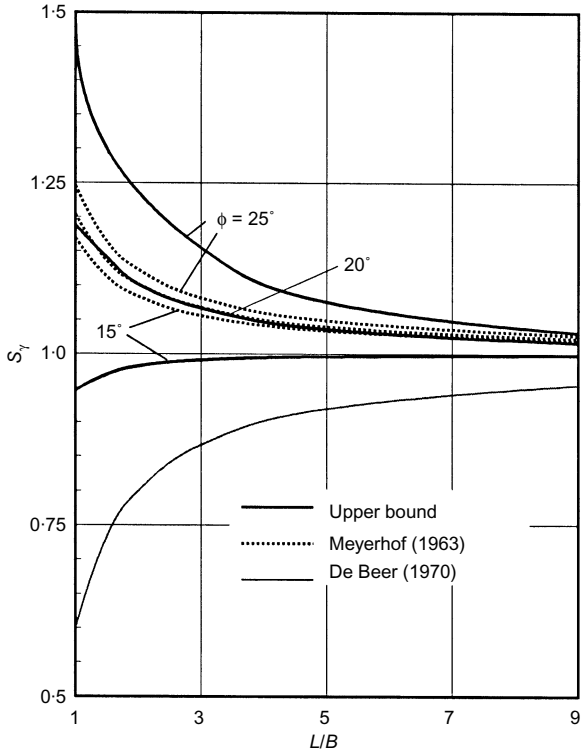

Fig. 9. Comparison of shape factors s_γ

consistent with small internal friction angle ($\varphi < 16°$), whereas Meyerhof's proposal reflects better the limit analysis solution for larger φ (the upper-bound solution and Meyerhof's s_γ are nearly identical for $\varphi = 20°$).

This is the first attempt at the rigorous limit analysis of rectangular footings on frictional soil. However, since no systematic experimental test results are available, validation of the shape factors derived cannot be done reliably. The results indicate that the existing proposals for shape factors are probably conservative. On the other hand, the factors obtained may be too optimistic.

Kinematical admissibility appears to be a significant constraint on the geometry of three-dimensional collapse mechanisms when compared with two-dimensional failure patterns. It was shown that in an n-block three-dimensional mechanism (with planar deformation) the number of free parameters with respect to which the geometry can be optimised is roughly half of that for a two-dimensional mechanism. Consequently, upper-bound estimates of limit loads for three-dimensional problems are likely to overestimate the true solutions by a larger margin (particularly for large φ) than estimates for two-dimensional problems. It is expected that an improvement in solutions for square and rectangular footings can be obtained by employing numerical techniques, such as FEM, which do not explicitly constrain the pattern of deformation. A separate issue is the application of the non-associative flow rule in upper-bound calculations. While a proposal by Drescher & Detournay (1993) would reduce (and therefore improve) the calculated limit loads, such solutions, while useful, could no longer be proved strict upper bounds.

An immediate benefit from this study is the theoretical development indicating that the tedious calculations of the work dissipation rate in the collapse mechanism can be effectively substituted by a much simpler surface integral. This is particularly important in solving three-dimensional problems, where the mechanism geometry can be quite complex. The mechanisms considered are elaborate but realistic, and their extension to other problems (such as three-dimensional slope stability and anchor plate pull-out) may prove to be useful.

ACKNOWLEDGEMENT

The work presented in this paper was supported by the National Science Foundation, grant No. CMS-0096167. This support is greatly appreciated.

APPENDIX 1

It is not feasible to present all the derivations related to constructing admissible three-dimensional mechanisms used in this paper. This Appendix gives only some indication as to how the rigid-block mechanism for a square footing was constructed. The mechanism consisting of rigid

blocks was found to be more adverse than the continuous deformation pattern, and the remarks below pertain to the former.

A velocity vector directed along the axis of a cone with apex angle of 2φ is inclined at φ to any plane tangent to the cone. Truncation of polyhedra with cones, as in Fig. 3, is then a convenient way to improve three-dimensional admissible mechanisms used in limit analysis. The mechanism in Fig. 3 was constructed starting from the pyramid under the footing. The inclination of the first cone was given by inclination angle α of the line of intersection of planes $A'O_1T_2'$ and $A''O_1T_2''$. This angle is shown in Figs 10(a) and 10(b). Once angle α is specified, angle 2ρ between the two planes (Fig. 10(b)) can be calculated as

$$\tan\rho = \frac{L}{B}\,\frac{\cos\beta_0}{\sin(\beta_0-\alpha)} \tag{20}$$

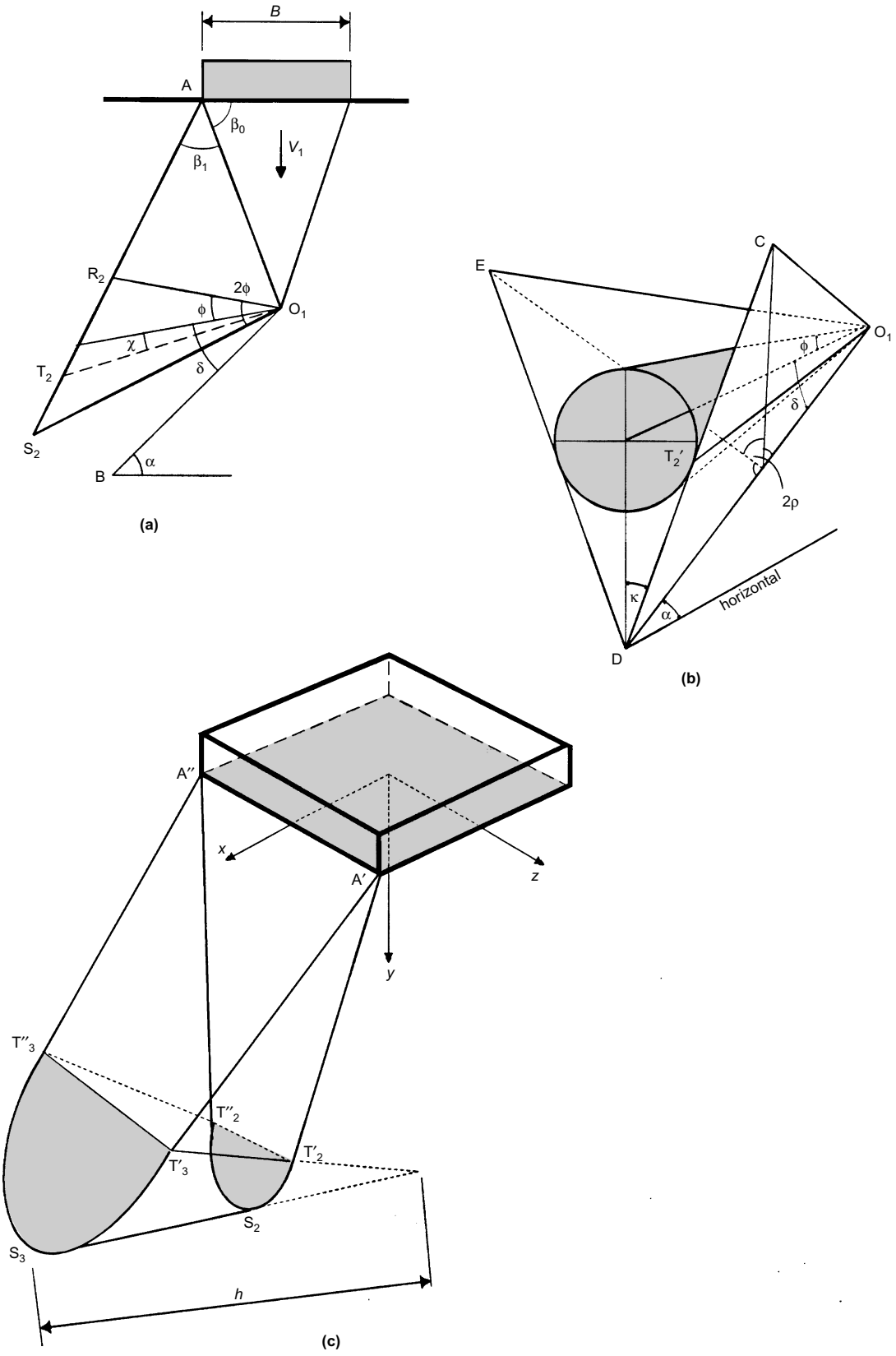

Fig. 10. Three-dimensional failure mechanism: (a), (b) construction of the first block; (c) rigid block truncated with a conical surface

where B and L are the width and length of the footing. Having determined angle ρ, the inclination of the cone axis is determined by angle δ:

$$\tan\delta = \frac{\tan\varphi}{\sin\kappa} \tag{21}$$

where angle κ is shown in Fig. 10(b), and is given implicitly in

$$\tan\kappa = \tan\rho\cos\left(\arctan\frac{\tan\varphi}{\sin\kappa}\right) \tag{22}$$

and the inclination of the projection of line O_1T_2' along which plane $A'O_1T_2'$ is tangent to the cone is given by

$$\tan\chi = \tan\varphi\sin\kappa \tag{23}$$

where angle χ is shown in Fig. 10(a) (angle between the cone axis and the projection of O_1T_2' on the plane of Fig. 10(a)). Once angle β_1 is specified, point T_2 and the location of the cone for the next block are uniquely determined (Fig. 4). Line $T_2'T_3'$, along which this next cone is tangent to the next plane, is found as a line intersecting points O_2 and T_2' (Fig. 3(a)):

$$\frac{x - x_O}{x_T - x_O} = \frac{y - y_O}{y_T - y_O} = \frac{z - z_O}{z_T - z_O} \tag{24}$$

where subscripts O and T denote the coordinates of points O_2 and T_2'. Point T_3' is then found as the point of intersection of the line in equation (24) and plane $A'S_3A''$ (Fig. 3(a)). This procedure was repeated until all blocks were generated.

Areas of the rupture surfaces were not calculated since it was shown in equation (5) that they are not needed for calculation of the work dissipation rate. Volumes of the blocks for calculations of the work rate of the soil weight were computed by dividing all the blocks into a triangular prism and a frustrum of a cone, with the directrix being a part of an ellipse (Fig. 10(c)). The volume of the prism in Fig. 10(c) is

$$V_{\text{prism}} = \tfrac{2}{3}S(T_3'T_3'' + T_2'T_2'' + A'A'') \tag{25}$$

where S is the area of the cross-section of the prism with plane $x - y$. The volume of the truncated cone i is

$$V_i^{\text{cone}} = \tfrac{1}{3}\left(\frac{2b}{a}\int_{a-k}^{a}\sqrt{a^2 - \xi^2}\,\mathrm{d}\xi\right)h - V_{i-1}^{\text{cone}} \tag{26}$$

where the expression in parentheses is the area bounded by the frustrum directrix (shaded part of an ellipse in Fig. 10(c)), a and b are the semi-axes of the elliptical directrix, and h is the cone height (Fig. 10(c)).

For rectangular footings, adjustments were made to accommodate a rectangular pyramid under the footing and a plane-strain insert as indicated in Fig. 5 (b).

REFERENCES

Bolton, M. D. & Lau, C. K. (1993). Vertical bearing capacity factors for circular and strip footings on Mohr–Coulomb soil. *Can. Geotech. J.* **30**, 1024–1033.

Caquot, A. I. (1934). *Équilibre des massifs á frottement interne. Stabilité des terres pulvérulentes et cohérentes*. Paris: Gauthier-Villars.

De Beer, E. E. (1970). Experimental determination of the shape factors and the bearing capacity factors of sand. *Géotechnique* **20**, No. 4, 387–411.

Drescher, A. & Detournay, E. (1993). Limit load in translational failure mechanisms for associative and non-associative materials. *Géotechnique* **43**, No. 3, 443–456.

Drucker, D. C. & Prager W. (1952). Soil mechanics and plastic analysis or limit design. *Q. Appl. Math.* **10**, No. 1, 157–165.

Golder, H. Q. (1941). The ultimate bearing pressure of rectangular footings. *J. Instn Civ. Engrs* **17**, No. 2, 161–174.

Hansen, J. B. (1970). A revised and extended formula for bearing capacity. *Geotek. Inst. Bull.* **28**, 5–11.

Leca, E. & Dormieux, L. (1990). Upper and lower bound solutions for the face stability of shallow circular tunnels in frictional material. *Géotechnique* **40**, No. 4, 581–606.

Meyerhof, G. G. (1963). Some recent research on the bearing capacity of foundations. *Can. Geotech. J.* **1**, No. 1, 16–26.

Michalowski, R. L. (1985). Limit analysis of quasi-static pyramidal indentation of rock. *Int. J. Rock Mech. Mining Sci.* **22**, No. 1, 31–38.

Michalowski, R. L. (1986). An approximate solution to a problem of pseudo-steady flow of strain-hardening material. *Int. J. Mech. Sci.* **28**, No. 4, 195–200.

Michalowski, R. L. (1997). An estimate of the influence of soil weight on bearing capacity using limit analysis. *Soils Found.* **37**, No. 4, 57–64.

Michalowski, R. L. (2001). The rule of equivalent states in limit state analysis of soils. *J. Geotech. Geoenviron. Engng* **127**, No. 1, 76–83.

Murray, E. J. & Geddes, J. D. (1987). Uplift of anchor plates in sand. *J. Geotech. Engng* **113**, No. 3, 202–215.

Prandtl, L. (1920). Über die Härte plastischer Körper. *Nachr. Königl. Ges. Wissensch., Göttingen; Mathematisch-physikalische Klasse*, 74–85.

Puzrin, A. M. & Randolph, M. F. (2001). On the superposition of plastically dissipated work in upper bound limit analysis. *Proc. Roy. Soc. Lond. Ser. A* **457**, 567–586.

Regenass, P. (1999). *Application de la méthode cinematique delanalyse limite au calcul de la butte tridimensionnelle et de la charge limite de plaques dancrage superficielles*. PhD thesis, Université Louis Pasteur, Strasbourg.

Reissner, H. (1924). Zum Erddruckproblem. In *Proc. First Int. Cong. Appl. Mech.* (eds C. B. Biezeno and J. M. Burgers), Delft, 295–311.

Shield, R. T. and Drucker, D. C. (1953). The application of limit analysis to punch-indentation problems. *J. Appl. Mech.* **20**, 453–460.

Terzaghi, K. (1943). *Theoretical soil mechanics*. New York: Wiley.

Vesic, A. S. (1973). Analysis of ultimate loads of shallow foundations. *J. Soil Mech. Found. Engng, ASCE* **99**, No. 1, 45–76.